Available online at www.sciencedirect.com

ScienceDirect

Solar Energy 116 (2015) 247–256

SOLAR ENERGY

www.elsevier.com/locate/solener

A proposed graphical electrical signatures supervision method to study PV module failures

Y. El Basri [a], M. Bressan [a,*], L. Seguier [a], H. Alawadhi [c], C. Alonso [a,b]

[a] CNRS, LAAS, 7 Avenue du Colonel Roche, F-31077 Toulouse, France
[b] Universite De Toulouse, UPS, INSA, LAAS, F-31400 Toulouse, France
[c] Department of Computer Science, Ehime University, Matsuyama, Japan

Received 11 September 2014; received in revised form 14 January 2015; accepted 13 February 2015

Communicated by: Associate Editor Bibek Bandyopadhyay

Abstract

The current literature has an important lack of knowledge on the various types of failures in terrestrial PV systems. This works seeks to remedy this issue by proposing a new method to detect failures based on simple electrical measurements. This helps to maximize the PV power production and to improve the knowledge of the environmental impact on premature failures. To validate this approach, this work proposes the analysis of numerous *I–V* curves under failure conditions. These curves are reproduced experimentally on a PV central, validating the proposed method.

Keywords: *I–V* curves analysis; Graphical electrical signatures; Shadow; Dust; Failure detection; Monitoring system

1. Introduction

In recent years, photovoltaic (PV) modules have become a popular source of energy in both commercial and residential applications. This energy source has received much attention as an alternative form of electricity generation and is currently present on buildings throughout the World. Most PV modules are silicon based, warranted for 25 years. However, it is difficult to find a complete PV conversion system, including electrical interfaces, with an equivalent lifetime in terrestrial applications. Furthermore, no accepted test protocol or monitoring exists to validate its lifetime. Globally, it is not easy to predict the degradation and aging linked to a geographic environment.

In the literature, PV modules present an overall efficiency degradation. Wohlgemuth quantifies an average annual degradation rate of 0.8% per year (Wohlgemuth and Kurtz, 2011). Other studies from Ndiaye et al. (2013), Solórzano and Egido (2013) or Ferrara and Philipp (2012) treat of many origins of degradations, aging and failures. Defects can be classified in different families in intern degradations and failures such as yellowing and browning of encapsulation material, delaminating and cracking of polymers used for encapsulates or back sheets caused by heat, humidity and UV irradiation. Some studies (Chamberlin et al., 2011; Ding et al., 2005) speak about the impact of these degradations and failures on the electrical characteristic of PV modules. It can change progressively with metal oxidation, discoloration of busbars and corrosion of connectors, increasing the series resistance of the

* Corresponding author.
E-mail addresses: yelbasri@laas.fr (Y. El Basri), michael.bressan@laas.fr (M. Bressan).

http://dx.doi.org/10.1016/j.solener.2015.02.048
0038-092X/

PV module. There are no methods to quantify these progressive effects, which renders the estimation of the origin of power losses and their real impact on the PV module degradation. This is a real challenge to the scientific community.

Several monitoring photovoltaic systems proposed in the literature try to identify different types of failures such as automatic supervision and fault detection procedure for PV systems, based on power losses analysis (Chouder and Silvestre, 2010; Villa et al., 2014). The fault analysis technique in this case is to compare predicted yields with real measured power output. For evaluating the efficiency of a PV plant, some studies (Ueda et al., 2006; Decker and Jahn, 1997) use variables such as the performance ratio. The performance ratio is the ratio of the actual and theoretically energy output and can give information concerning the behavior of a PV plant. In the study of Firth et al. (2010), the ratio of acquired data and reference data is classified into criteria range (shadow fault, inverter fault, component fault). According to this analysis, a failure is presumed to disturb PV efficiency, but this method is imprecise in detecting faults. In many cases, studies are based on simulation results and have not been implemented with real data, monitoring PV systems in real conditions (Chao et al., 2008).

The aim of this work was to create an automatic failure detection method based on the analysis of I–V curves. The proposed method is based on a gradient calculation and a Hessian calculation giving the shading area in function of the PV voltage or the PV current. The gradient calculation consists in calculating the first derivative and the Hessian calculation, the second derivative. The main objective of this detection was to accurately identify problems of some failures impacting the performance of PV modules such as soiling and oxidation.

This document is organized as follows; Section 2 presents the necessity to develop a model considering the effect of failures on I–V curves. Bishop's model (Bishop 1988) is used as a reference in this work. Section 3 presents the step of development of a sequential sampling board in order to obtain I–V curves of 6 PV modules. Section 4 speaks about a study of the major identified degradation and failure of PV modules such as yellowing and localized dust. As example, the effect of dust is shown and studied on DC power output and on I–V curves. Section 5 presents the fault detection method for evaluating some failures impact on PV modules performed by the gradient calculation and the Hessian calculation. Simulation and experimental tests are described showing performances of the fault detection.

2. I–V model description

When a PV module is partially shaded, some of its cells can be forced to work in reverse bias. To avoid this, most commercial PV modules are equipped with bypass diodes that, when biased, change the I–V curves of the PV modules. As a result, it is essential to have a PV cell model capable of characterizing the effect of the reverse bias when solar cells are shaded. Several researchers have proposed a mathematical model of a PV module to simulate its characteristic according to the effect of the temperature and the solar irradiation (Walker, 2001; Villalva et al., 2009). However, most of the models in the literature do not take into account the effect of the reverse bias. The only exception is the model proposed by Bishop, (1988) which incorporates the avalanche effect as a non-linear multiplication factor that affects the shunt resistance current term, shown below:

$$I = I_{ph} - I_0\left[\exp\left(\frac{(q(V + I\cdot R_s))}{nkT}\right) - 1\right] - \frac{V + I\cdot R_s}{R_{sh}} \times \underbrace{\left[1 + a\left(1 - \frac{V + R_s\cdot I}{V_{br}}\right)^{-m}\right]}_{\mathrm{M(V1)}} \quad (1)$$

where I_{ph} is the photocurrent (A), I_0 is the dark saturation current (A), n is the ideality factor of the diode (1–2), k is the Boltzmann constant ($1.38\cdot 10^{-23}$ J/K), q is the magnitude of the electron charge ($1.602\cdot 10^{-19}$ °C), T is the temperature of the cell (°C), R_s is the series resistance (Ω), R_{sh} the shunt resistance (Ω), a and m are constant, and V_{br} is the avalanche breakdown voltage (V). The equivalent circuit of Eq. (1) is shown in Fig. 1.

The additional term, M(V1), is added to the leakage current into the shunt resistance term modeled as a controlled current source. The shading effect may be represented through the variation of some parameters in the circuit shown in Fig. 1. First, using Newton–Raphson method and Eq. (1), all PV cell parameters are obtained as shown in Table 1.

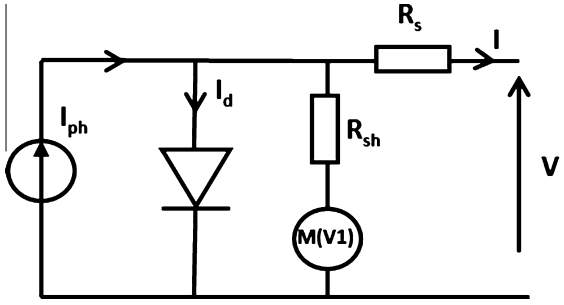

Fig. 1. The equivalent circuit of solar cells.

Table 1
Parameters used in this work.

Parameter	Value	Bishop's term	Value
I_0	$1.55\cdot 10^{-5}$ A	V_{br}	−15 V
n	1.486	a	0.001
R_{sh}	9 Ω	m	3
R_s	9 mΩ		
T	25 °C		

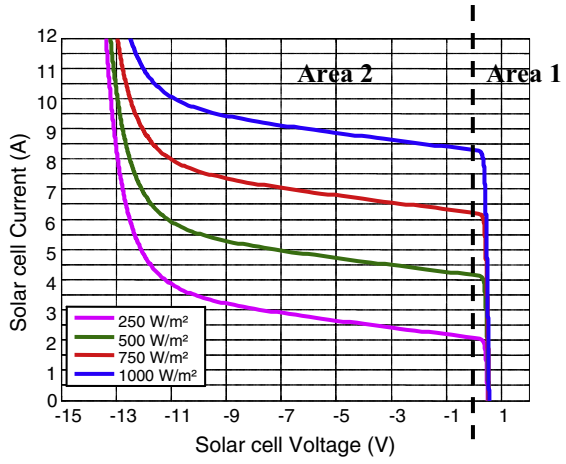

Fig. 2. *I–V* curves of a PV cell working under different irradiance levels.

As an example of simulation, *I–V* curves of a PV cell obtained using the model above and the parameters from Table 1 are shown in Fig. 2. The same approach can be used to model an entire module.

In Fig. 2, the area 1 corresponds to electrical characteristic of the PV cell in normal operating conditions when the solar cell produces power. The PV cell operates in area 2 when the current flowing through the solar cell is higher than its short-circuit current. The cell is then forced in reverse bias, consuming power. The PV cells risks destruction if its voltage reaches breakdown values. As a conclusion, it is essential to study *I–V* curves when failures such as soiling and oxidation are detected.

3. PV field sampling

In order to acquire *I–V* curve and to save it in an independent database, a sequential sampling board was developed for measuring 6 PV panels using a capacitor allowing to change the voltage from 0 V to V_{oc}. The principle of this board is to acquire the current and the voltage during the charge of the capacitor. Each PV module is connected to a multiplexer switch which drives the PV current to the circuit sensor. The structure shown in Fig. 3 is composed of two switches IRF2807Z control by a TC4420 Mosfet driver: T1 starting the charge of the capacitor and T2 managing the discharge through the resistor *R* in order to limit the discharge current. Voltage (*V*) and current (*I*) are measured reciprocally through a resistive bridge and through a shunt resistor. Data are scanned by a microcontroller (dsPCI30f1010). The resolution of the integrated analog to digital converter is 10 bits with a conversion rate of 2 Msp, which gives an accuracy of ±20 mV and ±5 mA.

Two Mosfet transistors IRF2807Z associated with a high voltage isolated MOSFET driver (HT0740) are used to connect the desired PV panel to the sampling circuit. This configuration is used in the positive and negative way in order to electrically isolate the module. It is because the intrinsic embedded diode of the power Mosfet will be allowed a reverse current to pass into the other modules (Fig. 4).

Fig. 5 presents the sampling board prototype composed of the microcontroller, the sampling switch (T1 and T2) with the capacitors and the multiplexor switch which allows activating the characterization of the desired PV

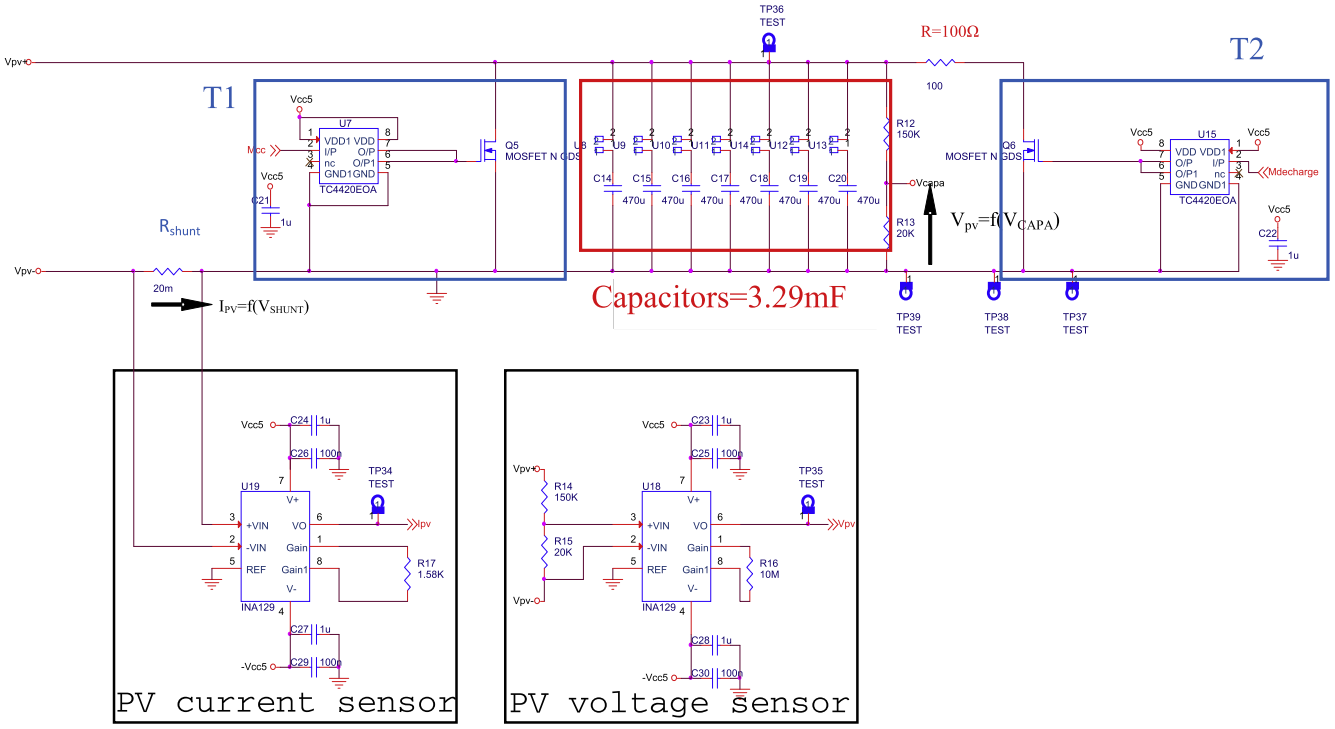

Fig. 3. Electrical schema of the sampling circuit based of the charge of a capacitor.

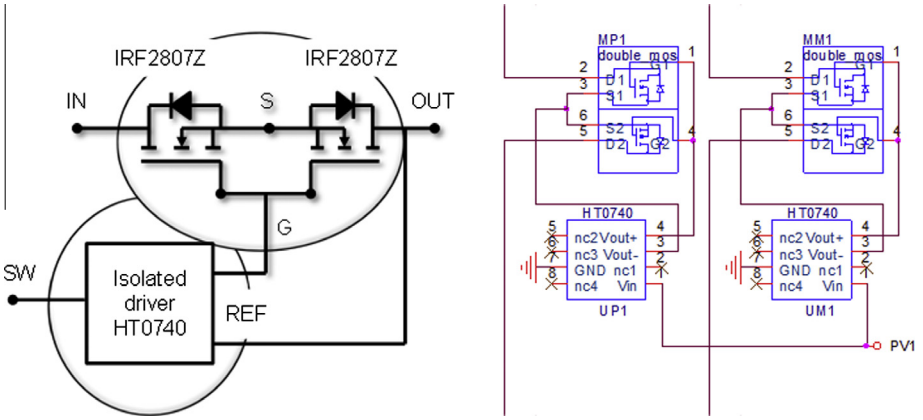

Fig. 4. Switch multiplexor.

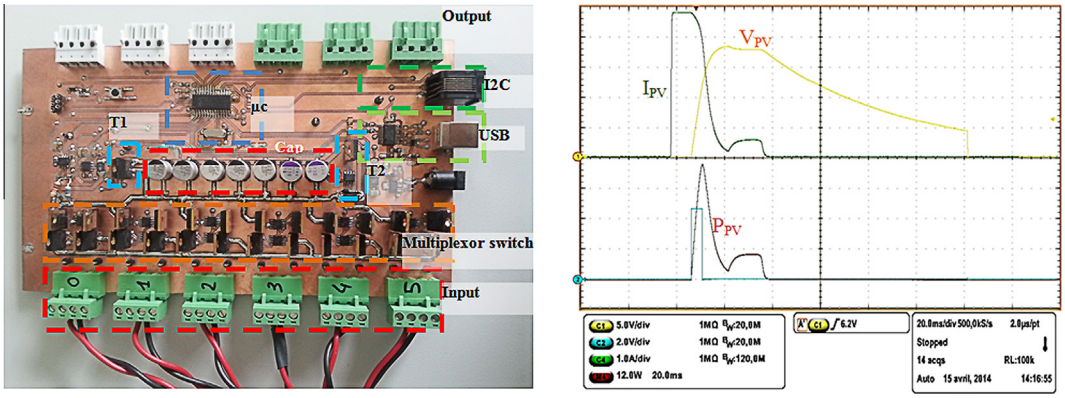

Fig. 5. Sampling board I_{PV} (V_{PV}) and P_{PV} for 6 PV panels.

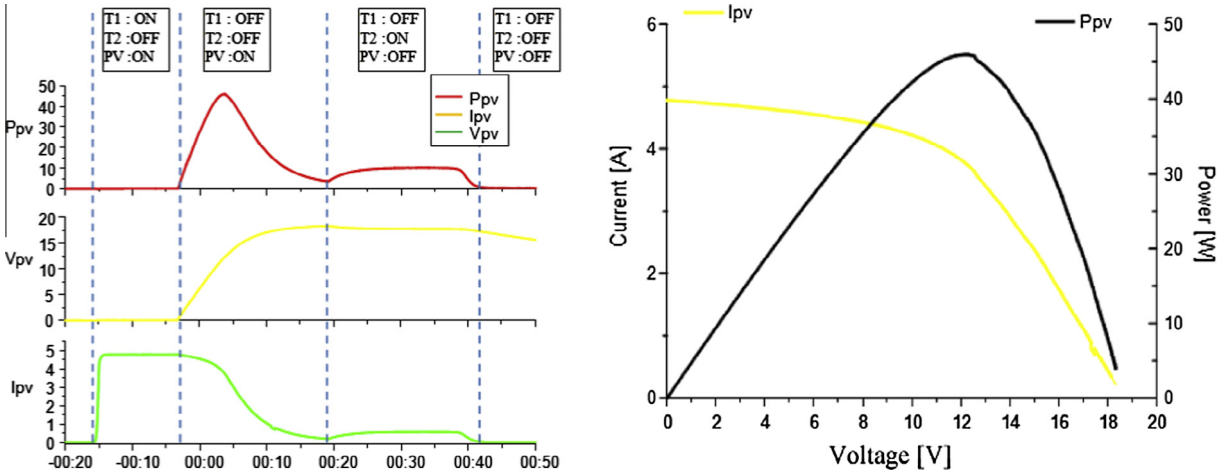

Fig. 6. Sampling result of a PV module.

panel. Finally I2C and USB communications are used to communicate with an embedded system or directly with a computer. The consumption of the prototype is around 0.5 W.

Fig. 6 shows the experimental measurement on the oscilloscope of the current (I_{PV}), the voltage (V_{PV}), the power (P_{PV}) signals and the signature of the power derivative.

Depending on the current provided by the PV module, the time required for the characterization is around 160 ms. The power lost during this period must be taken into account in the final detection computation.

4. Study of electrical impact of degraded PV modules

Once the *I–V* model described and the *I–V* tracer developed, it is now essential to describe the major known degradations and failures of a PV module. Each failure has a specific effect on the electrical characteristic of PV modules. As an example, the effect of dust on PV modules modifies the shape of the *I–V* curves and PV module efficiency can decrease if the dust continues to accumulate over it.

4.1. Context

A list of the major known degradations and failure of PV modules as described on several studies such as (Ndiaye et al., 2013; Solórzano and Egido, 2013) is given in Table 2.

Until now, the literature has no direct relation between measured power losses and their physical origin. Nevertheless, each fault has a specific effect on the electrical characteristic of PV modules, such as increasing the series resistance, resulting on one or more alterations on its *I–V* curve. For example, defects of a group of PV cells, such as micro cracks, cell breakage and hot spots, have a higher impact on the performances and can be easily detected through *I–V* curves. However, it is globally difficult to know if the power losses are due to PV module degradation or other causes external to PV systems as shading.

Thus, the diagnosis of the origin of failures and their types of signatures on *I–V* curves is not easy in many cases. This study work is focused on the main parameters of *I–V* curves that allow for cross comparison studies. The main parameters of a PV module in this work are as follows: the short-circuit current (I_{sc}), the open-circuit voltage (V_{oc}), the maximum power (P_{max}) and the fill factor (FF). These main characteristics are directly linked to the quality of energy conversion capability at the existing conditions of irradiance and temperature. For each fault, the shape of the *I–V* curve presents different changes in comparison with the reference condition (normal operation).

Table 2
Modes of crystalline silicon degradation and failure.

PV modules	Degradation	Failure
Crystalline PV modules	Yellowing/browning of encapsulants	Shading
	Interconnection broken	Irregular dust
	Broken cells	Localized dust
	Corrosion	
	Delamination of the encapsulant	
	Broken glass	
	Hot spot	
	Bypass diode defects	

In the next part, an example of shading linked to a deposited dust is treated in order to see the behavior of the *I–V* curve and try to discover a systematic identification of this type of fault.

4.2. The effect of dust on PV modules

The accumulation of dust on the surface of PV plant reduces the glass cover transmittance, hence decreases the amount of solar irradiation reaching the cells (Adinoyi and Said, 2013). In terrestrial PV systems, this accumulation on the active surface area of a PV module progressively decreases the PV power supplied. Some authors (Kimber et al., 2006; Mejia et al., 2014) estimate these losses to be an average of 0.05% per day of the PV plant global total power. For 26% of the sites presenting roofs with tilt angles less than 5°, losses can be greater than 0.1% per day. To quantify the effect of dust on PV modules, two PV modules exposed to an urban environment and tilted 10° south facing were monitored. One module is cleaned regularly while the other is not. The initial modules specifications are shown in Table 3.

The impact of the *I–V* curve and the difference on shape between a regular cleaned module and the other with dust is shown in Fig. 7. In this figure, it is essential to compare the measurements of *I–V* characteristics performed by the PV sampling board and the *I–V* model in order to validate the work explained in Sections 2 and 3.

Another, impact of soiling and dust PV modules is the formation of hotspots (Herrmann et al., 1997). As a result, hot spots phenomena can be one of consequences of a long period of dust deposition. In Fig. 7, *I–V* curves, measured in very clear conditions (950 W/m^2) are shown. The two *I–V* curves in Fig. 7(a) represent the PV module with irregular dust and two *I–V* curves in Fig. 7(b) show the clean PV module. Their cross-comparison shows that the dust impacts the *I–V* curve of the PV module by activating one of its bypass diode.

For evaluating *I–V* model performances, the mean relative error (MRE) is used for the both cases (a) and (b). This relation is given by:

$$\mathrm{MRE} = \sum_{i=1}^{N} \frac{(y_i - x_i)}{x_i} / N \tag{2}$$

Table 3
PV modules specifications.

Manufacturer	TE2200
Cell type	Mono crystalline
Maximum power rating (P_{max})	240 Wp
Open circuit voltage (V_{oc})	37.2 V
Short circuit current (I_{sc})	8.6 A
Voltage at maximum power (V_{mp})	29.6 V
Current at maximum power (I_{mp})	8.2 A
Temperature coefficient of current (α)	+4.8 mA/°C
Temperature coefficient of voltage (β)	−129 mV/°C
Temperature coefficient of power (Ψ)	−0.43 %/°C
Diodes	3 bypass

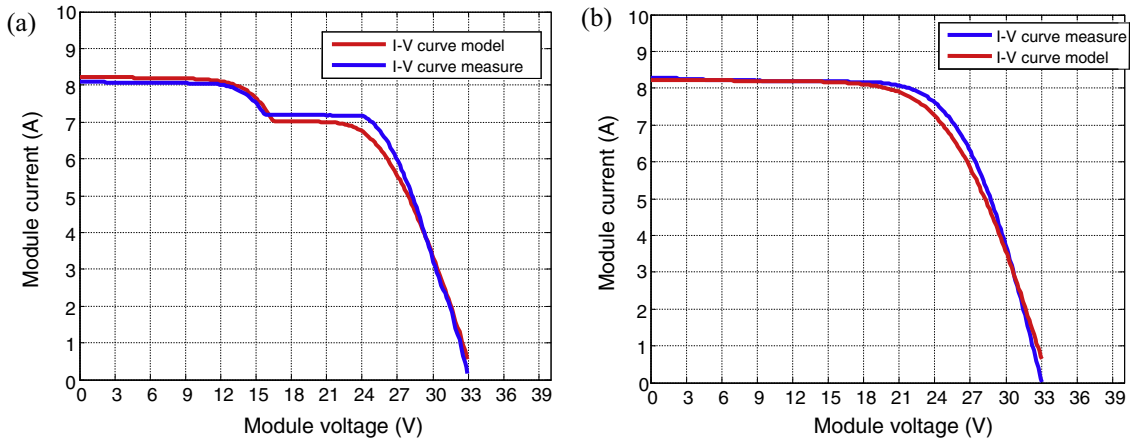

Fig. 7. *I–V* curves measured and modeled for a dusty PV module (a) and for a clean PV module (b).

Table 4
Mean relative error of a clean PV module and a dusty PV module.

PV modules	MRE
Dusty PV module (model/measure)	5.57%
Clean PV module (model/measure)	1.88%

where y_i is the ith modeled voltage value, x_i is the ith measured voltage, and N being the number of data analyzed. The several errors results are shown in Table 4.

These results can be considered satisfactory for the next study and the fault detection presented in the next part.

5. Fault detection based on gradient and Hessian calculation

I–V curves can change significantly when soiling or dust is present over PV modules. Moreover, their presence can also cause the PV performances to decrease on the long-term. It is important, thus, to develop a fault detection based on the analysis of *I–V* curves acquired during failure operating conditions. This work proposes a detection method based on the first derivative calculation (gradient) and the second derivative calculation (Hessian), as explained below.

5.1. Gradient and Hessian model

The method presented in this paper is based on the analysis, through two methods, of *I–V* curves acquired under degraded operating conditions.

The first method is called the gradient method and uses the following equations to calculate the first derivative for *I–V* curves:

$$\frac{DI}{DV} = \frac{I(t+1) - I(t)}{V(t+1) - V(t)} \tag{3}$$

The second method is called the Hessian method and uses the following equation to calculate the second derivative of the *I–V* curves:

$$\frac{D^2I}{DV^2} = \frac{\frac{DI}{DV}(t+1) - \frac{DI}{DV}(t)}{V(t+1) - V(t)} \tag{4}$$

The first derivative is used to identify the fault type and the second derivative is used to tell different faults of the same type apart. The next section will illustrate their use through the simulation of some typical fault scenarios.

5.2. Simulation scenarios of failure on PV module and results of the fault detection

The failure scenarios simulated in this part will help understand the effect of each failure on *I–V* curves. The results from these simulations will provide the bases for the experimental validation of the proposed detection method. Moreover, this will ensure to differentiate each default presented in this part. The PV modules specifications shown in Table 3 are used to simulate many *I–V* curves. A solar cell is represented by the model shown in Fig. 1.

Certain failures have an impact directly over specific cell parameters. For example, dust or soiling can activate the bypass diodes while parallel high conductivity shunts across the P-N junction of the cell affect the often neglected shunt resistance (R_{sh}) (Meyer and van Dyk, 2005). Conversely, anything affecting the cell solder bonds, the emitter and base regions, the cell metallization, the cell interconnect busbars or the resistances of the junction-box terminations will affect the series resistance (R_s) of the model.

Five failure simulation scenarios are proposed in Fig. 8. They are all based on changes made to the module parameters described above.

- Case 1 shows the *I–V* curve when PV modules operate in classical working conditions, considered as reference.
- Case 2 represents an increase of the series resistance, causing a deviation of the curves around the open circuit voltage region.

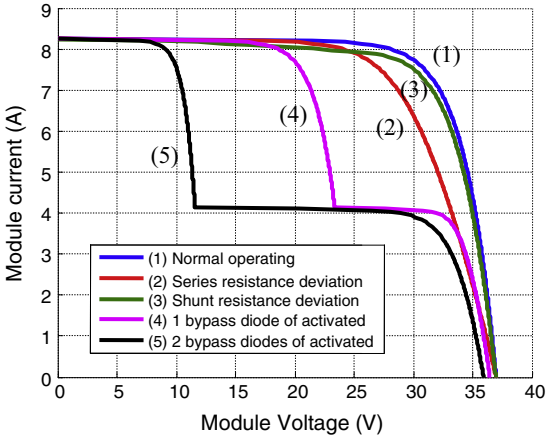

Fig. 8. *I–V* curves simulation with four major failures.

- Case 3 represents a problem on the junction of the PV cells causing their shunt resistance to decrease.
- Case 4 represents the case where one of three bypass diodes of the PV module studies is activated.
- Case 5 represents the case where two of three bypass diodes of the PV module studies are activated.

On these *I–V* curves, the behavior of all the simulated characteristics differs according to the failures. As a result, an electrical failure signature can be identified for purpose of fault detection and identification. The gradient calculation and the Hessian calculation can help to differentiate all simulated defects. The main result of these analyses is shown in Fig. 9.

The gradient calculation can provide some information according to each *I–V* curves. In Fig. 9(a), several negative peaks appear related to the activation of bypass diodes. When one of three bypass diodes is activated (4), the negative peak is situated around 23 V while for the case of two bypass diodes of activated (5), the negative peak is around 12 V.

When the series resistance increases, the shape of the gradient curve (2) is different compared to the shape of the gradient curve in normal operating (1). Moreover, its minimum negative value tends toward −1.5 A/V, contrary to the minimum negative value of the gradient curve in normal operating which tends toward −3.0 A/V. Thus, observing the minimum negative value can be a good indicator to differentiate a problem on the series resistance.

Concerning the shunt resistance, the shape of the gradient curve (3) is not much different than the curve in normal operating. The difference is visible for the minimum negative value but it is not significantly. Thus, the gradient calculation allows the identification of series resistance variation but it is not sufficient to detect changes in the shunt resistance.

The Hessian method can clearly distinguish the activation of one or more bypass diodes. In it, a sign change occurs from negative to positive every time a diode is activated, as shown in Fig. 9(b). A positive peak appears around 12 V and 23 V meaning the activation of one or more bypass diodes. Since all other values are negative or tend toward zero, these peaks can be easily detected by automatic algorithms. The second derivative of the shunt resistance (3) shows a small difference with the curve in normal operating. It is difficult to interpret a deviation in this case.

This simulation validates the fault detection method and it is essential to proceed at experimental tests.

5.3. Experimental test scenarios of failure on a PV module and results of the fault detection

The experimental test scenarios proposed in this subsection will validate the fault detection proposed in the previous one. However, only shading test scenarios are performed due to the difficulty of realistically changing the series resistance. For each shading test, the *I–V* curves are given in Fig. 10(b).

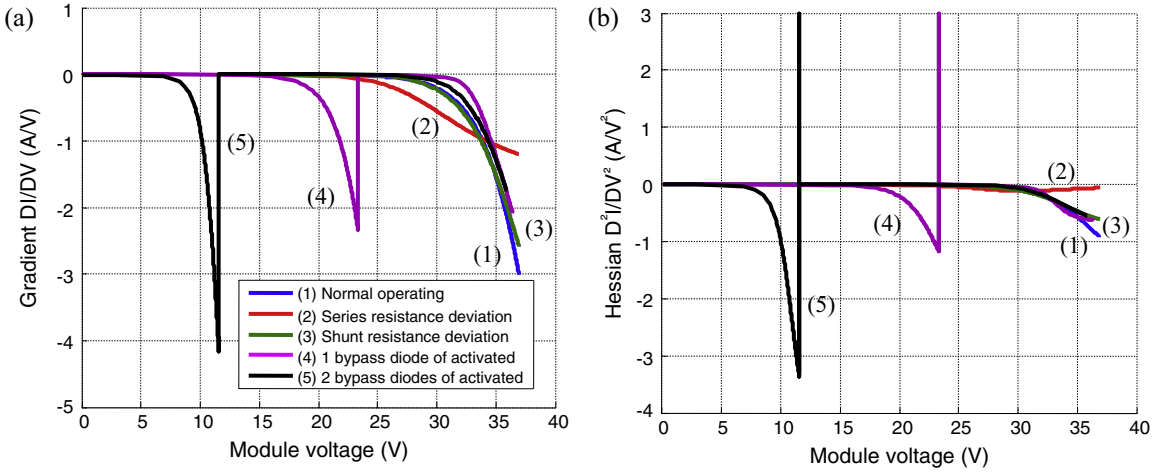

Fig. 9. Gradient on *I–V* curves (a) and Hessian on *I–V* curves (b) in simulation.

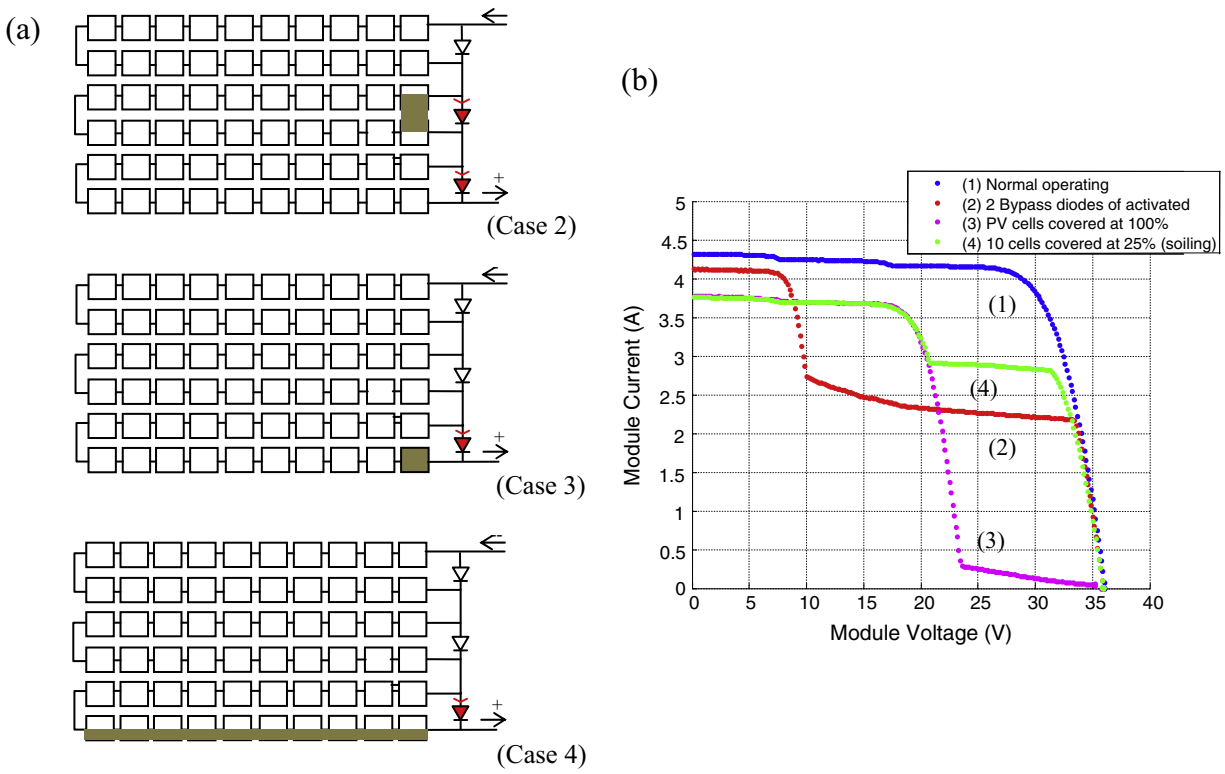

Fig. 10. Experimental test on PV module (a) and *I–V* curves for each test scenario (b).

The experimental tests performed on the PV module are shown in Fig. 10(a). Its equivalent *I–V* curves are shown in Fig. 10(b). Each case is described in detail below.

- Case 1 shows *I–V* curve in normal operating.
- Case 2 presents two covered cells at 50% of two different groups of PV cells in PV module.
- Case 3 is the case when a PV cell is totally covered causing the activation of the bypass diode.
- Case 4 shows homogeneous soiling of a group of cells of PV module.

From Fig. 10(b), it is important to note that the shading tests modify the shape of *I–V* curves because of the activation of one or more bypass diodes. For each shading test, this bypass diode activation introduces one step on *I–V* curves. Each step corresponds to a different shading area.

The results of the fault detection with the gradient and the Hessian calculations are shown respectively in Fig. 11(a) and (b).

For the shading experimental tests on the PV module, the gradient calculation validates the simulation performed in the previous part. From Fig. 11(a), when one or more

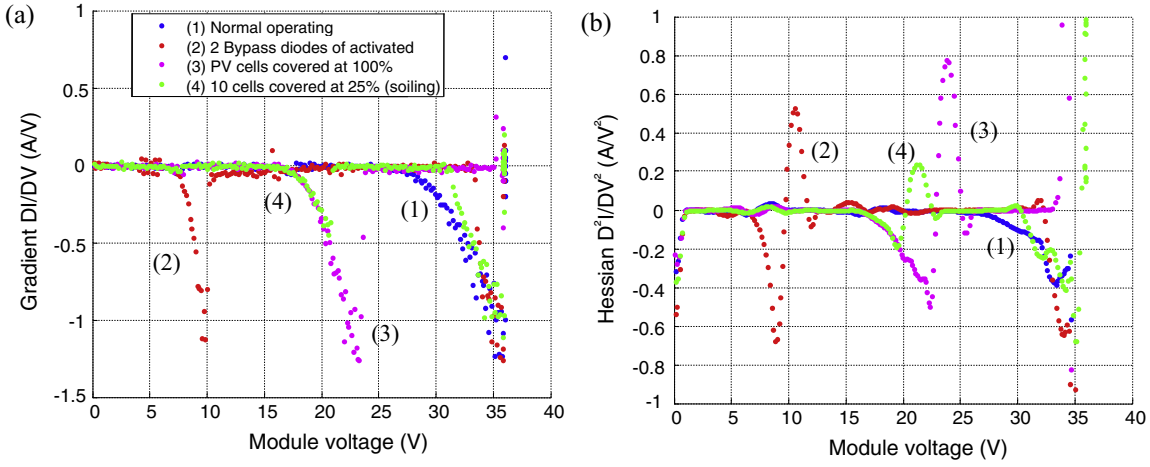

Fig. 11. Gradient on *I–V* curves (a) and Hessian on *I–V* curves (b) for experimental test scenarios.

bypass diode are activated, the negative peak has a strategically position in function of the PV module voltage but it is not sufficient to distinguish clearly each shading test.

In the Hessian case, to ease the interpretation of the results, the *I–V* curves were smoothed. There are positive peaks around 12 V, 22 V and 24 V such as the position of the PV module voltage for the *I–V* curve in Fig. 10(b). The number of activated bypass diodes validates the work of fault detection and the problem of shading on PV module causing performance loss.

Based on this analysis, it is possible to develop a simple algorithm capable of detecting the shading problem. This algorithm could inform PV users or manufacturers of failure over PV modules. An *I–V* structured flowchart for detecting failures according to this previous analysis is proposed in Fig. 12.

From Fig. 12, the first step of this algorithm is to perform the measurement of the *I–V* curve of the PV module. The next step consists in calculating the gradient and the Hessian of the *I–V* curve for analysis.

The first verification is the minimum value of the gradient around V_{oc}. If there is an increase in series resistance, the behavior of the gradient curve changes compare to the gradient curve in normal operation. Moreover, the minimum negative value is different evaluated at −1.5 A/V contrary to the value of the gradient curve in normal operation which is at −3 A/V. As a result, if the minimum negative value around V_{oc} does not go below −1.5 A/V then a series resistance deviation is confirmed.

The second verification concerns the maximum value issued from the Hessian analysis. Any value higher than zero can be used to deduce the number of active bypass diodes, depending on the PV voltage value where it occurs.

Concerning the shunt resistance, it is difficult to dissociate a deviation with this analysis. As a result, the proposed method cannot, however, detect any changes in the shunt resistance.

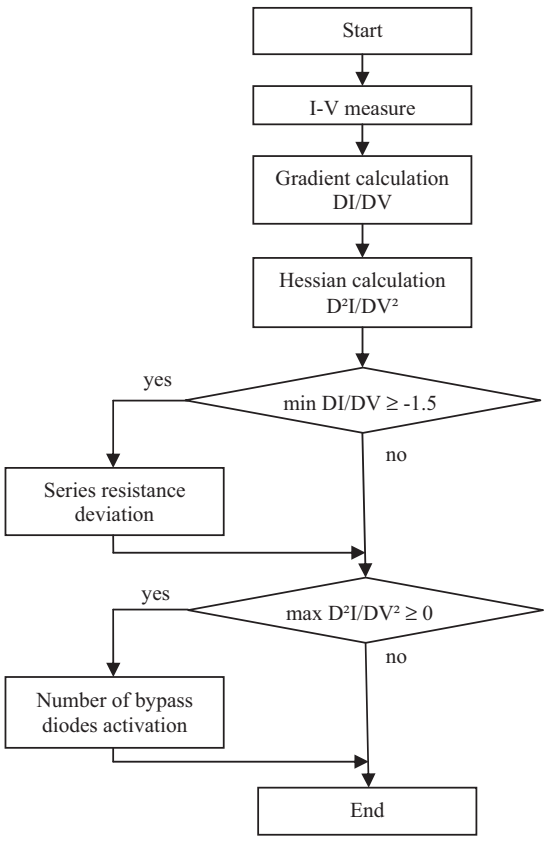

Fig. 12. Gradient and Hessian calculation and fault detection.

6. Conclusion

The current literature lacks an overall method capable of detecting different kind of defaults in PV plants. This work has proposed a method for detecting defaults in PV plants based on the analysis of *I–V* curves acquired during normal and faulty operating conditions. The method is based on the analysis of the first and second derivative of the current of the *I–V* curve in relation to the voltage. The first derivative is used to detect defects over the series resistance while the second derivative is used to detect the activation of bypass diodes. The method is explained, simulated and its results are validated experimentally. This method can be used by manufacturers to monitor the conditions of PV plants and detect any changes in its parameters over time as well as the activation of bypass diodes due to shading.

References

Adinoyi, M.J., Said, S.A.M., 2013. Effect of dust accumulation on the power outputs of solar photovoltaic modules. Renew. Energy 60, 633–636.

Bishop, J.W., 1988. Computer simulation of the effects of electrical mismatches in photovoltaic cell interconnection circuit. Commission of the European Communities Joint Research Centre, ESTI Project.

Chamberlin, C.E., Rocheleau, M.A., Marshall, M.W., 2011. Comparison of PV module performance before and after 11 and 20 years of field exposure. In: Photovoltaic Specialists Conference (PVSC), 2011 37th IEEE, pp. 101–105.

Chao, K.H., Hob, S.H., Wanga, M.H., 2008. Modeling and fault diagnosis of a photovoltaic system. Electric Power Syst. Res. 78, 97–105.

Chouder, A., Silvestre, S., 2010. Automatic supervision and fault detection of PV systems based on power losses analysis. Energy Convers. Manage. 51, 1929–1937.

Decker, B., Jahn, U., 1997. Performance of 170 grid connected PV plants in Northern Germany—analysis of yield and optimization potentials. Sol. Energy 59, 127–133.

Ding, J., Cheng, X., Fu, T., 2005. Analysis of series resistance and *P–T* characteristics of the solar cell. Vacuum 77, 163–167.

Ferrara, C., Philipp, D., 2012. Why do PV modules fail? Energy Proc. 15, 379–387.

Firth, S.K., Lomas, K.J., Rees, S.J., 2010. A simple model of PV system performance and its use in fault detection. Sol. Energy 84, 624–635.

Herrmann, W., Wiesner, W., Waassen, W., 1997. Hot spot investigations on PV modules-new concepts for a test standard and consequences for module design with respect to bypass diodes. In: Proceedings of the 26th IEEE Photovoltaic Specialists Conference, pp. 1129–1132.

Kimber, A., Mitchell, L., Nogradi, S., Wenger, H., 2006. The effect of soiling on large grid-connected photovoltaic systems in california and

the southwest region of the united states. In: Photovoltaic Energy Conversion, Conference Record of the 2006 IEEE 4th World Conference, vol. 2, pp. 2391–2395.

Mejia, F., Kleissl, J., Bosch, J.L., 2014. The effect of dust on solar photovoltaic systems. Energy Proc. 49, 2370–2376.

Meyer, E.L., van Dyk, E.E., 2005. The effect of reduced shunt resistance and shading on photovoltaic module performance. In: Photovoltaic Specialists Conference.

Ndiaye, A., Charki, A., Kobi, A., Kébé, C.M.F., Ndiaye, P.A., Sambou, V., 2013. Using ons of silicon photovoltaic modules: a literature review testing to predict module reliability. Sol. Energy 96, 140–151.

Solórzano, J., Egido, M.A., 2013. Automatic fault diagnosis in PV systems with distributed MPPT. Energy Convers. Manage. 76, 925–934.

Ueda, Y., Kurokawa, K., Itou, T., Kitamura, K., Yokota,M., Sugihara, H., 2006. Performance ratio and yield analysis of grid connected clustered PV systems in Japan. In: Photovoltaic Energy Conversion, Conference Record of the 2006 IEEE 4th World Conference, pp. 2296–2299.

Villa, L.F.L., Raison, B., Crebier, J.C., 2014. Toward the design of control algorithms for a photovoltaic equalizer: detecting shadows through direct current sampling. IEEE J. Emerg. Sel. Top. Power Electron. 2, 893–906.

Villalva, M.G., Gazoli, J.R., Filho, E.R., 2009. Comprehensive approach to modeling and simulation of photovoltaic arrays. IEEE Trans. Power Electron. 24 (5).

Walker, G., 2001. Evaluating MPPT converter topologies using a MATLAB PV model. J. Electr. Electron. Eng. Aust. 21 (1), 49–56.

Wohlgemuth, J.H., Kurtz, S., 2011. Using accelerated testing to predict module reliability. In: Photovoltaic Specialists Conference (PVSC), 2011 37th IEEE, pp. 3601–3605. (NREL).